

Pair plasma cushions in the hole-boring scenario

J.G. Kirk¹, A.R. Bell^{2,3}, C.P. Ridgers^{3,4}

¹ Max-Planck-Institut für Kernphysik, Heidelberg, Germany

² Clarendon Laboratory, University of Oxford, Oxford, UK

³ Central Laser Facility, STFC Rutherford-Appleton Laboratory, Chilton, UK

⁴ Department of Physics, University of York, York, UK

Abstract. Pulses from a 10 PW laser are predicted to produce large numbers of gamma-rays and electron-positron pairs on hitting a solid target. However, a pair plasma, if it accumulates in front of the target, may partially shield it from the pulse. Using stationary, one-dimensional solutions of the two-fluid (electron-positron) and Maxwell equations, including a classical radiation reaction term, we examine this effect in the hole-boring scenario. We find the collective effects of a pair plasma “cushion” substantially reduce the reflectivity, converting the absorbed flux into high-energy gamma-rays. There is also a modest increase in the laser intensity needed to achieve threshold for a non-linear pair cascade.

PACS numbers: 12.20.-m, 52.27.Ep, 52.38.Ph

Accepted for publication in *Plasma Phys. Control. Fusion*

1. Introduction

Particle-in-cell simulations of ultra-intense laser pulses interacting with plasma now probe the regime in which non-linear QED processes are important [1, 2, 3], and predict the production of large numbers of gamma-rays and electron-positron pairs when the laser interacts with either an over-dense or an under-dense plasma. Next generation lasers (10 PW) will be able to test these predictions. However, it is still not clear whether or not the fully non-linear pair cascade predicted by Bell & Kirk [4] and Fedotov et al [5] will be achieved. For counter-propagating pulses, the threshold is expected to lie below a single pulse intensity of 10^{24} W cm⁻². But simulations of interactions with over-dense plasmas [2], which are the more straightforward experimental set-up, have identified several effects that might raise the required threshold intensity.

One effect with similar consequences that has so far not been analyzed is the screening by a cloud or “cushion” of pair plasma in the laser pulse just ahead of the target. As this cushion approaches the critical density, collective effects in the pair plasma can be expected to slow down the laser pulse and reflect or absorb it. Such cushions are observed in PIC simulations of linearly polarized laser pulses interacting with dense, solid targets (see, for example, figure 1 in [2]), but their dynamics are complex. In this paper we do not attempt an analysis of simulation results. Instead,

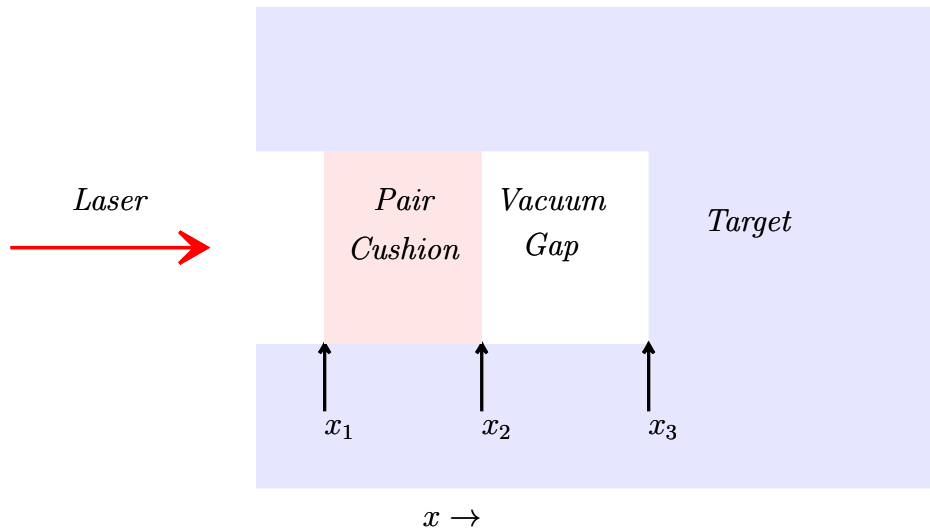


Figure 1. Sketch of the idealized hole-boring scenario. A pair cushion is located in the laser beam at $x_1 < x < x_2$. Note that a vacuum gap, at $x_2 < x < x_3$, must separate the cushion from the hole-boring front.

we try to gain a qualitative understanding of pair cushions by investigating stationary solutions in a highly simplified situation. Although they might be difficult to realize in practice, these solutions provide an easily quantifiable framework in which to interpret PIC simulations and discuss experimental set-ups.

We consider the interaction of a circularly polarized laser beam with a solid target in the hole-boring scenario [6, 7, 8], as sketched in Fig. 1. A pair plasma cushion, located in the region excavated by the beam, is described by a one-dimensional, cold, two-fluid model that includes a classical radiation reaction term. Stationary solutions are found and matched to the boundary conditions of the incoming laser beam on one side, and the standing wave in the vacuum gap, on the other. Section 2 describes the hole-boring scenario and, in particular, the relativistic dynamics of the hole-boring front; section 3 presents the two-fluid equations and the method of their solution in the rest frame of the hole-boring front; section 4 analyzes the properties of these solutions and section 5 discusses a practical application. We conclude with a discussion of the physical significance of the solutions.

2. The hole-boring scenario

2.1. Dynamics of the hole-boring front

The one-dimensional model of hole-boring by a circularly polarized plane wave is based on the properties of the “hole-boring front” [6, 7, 8] that divides the vacuum waves on one side from the high density plasma (originally solid) on the other. The front reflects the ions and electrons that stream into it as it advances into the solid, by means of a

charge-separated region that supports a strong, longitudinal electric field. At the same time, the front perfectly reflects the circularly polarized laser that is incident on its other surface. A closer look reveals that electrons are absent in the charge-separated region, which is bounded on the target side by an “electron sheath”, a thin enhancement in the electron density at which the laser is reflected. The target ions stream in through the electron sheath, are brought to rest by the longitudinal electrostatic field, and subsequently accelerated back through the electron sheath [7]. The key parameter in this scenario is the ratio of the incident laser intensity I^+ , assumed be a circularly polarized, monochromatic plane wave of (angular) frequency ω_{lab} propagating in the positive x direction, and the solid target density ρ (both measured in the lab. frame), which are combined into the dimensionless quantity

$$\begin{aligned} X &= I^+ / (\rho c^3) \\ &= 0.37 \times \left(\frac{I^+}{10^{24} \text{ W cm}^{-2}} \right) \left(\frac{\rho}{1 \text{ g cm}^{-3}} \right)^{-1} \end{aligned} \quad (1)$$

For a laser pulse of intensity $I^+ < 10^{24} \text{ W cm}^{-2}$ impacting a metal target, $X \ll 1$. The thickness of the charge-separated region is then approximately $\sqrt{X}c/3\omega_i$ [7], where ω_i is the ion plasma frequency in the fully ionized target. This length is small compared to the laser wavelength, which is the characteristic dimension of the pair cushion. Therefore, we will treat the hole-boring front as a singular surface current — a perfect mirror, at which the electric field vanishes.

The speed of advance of the front into the solid, as well as the energy in the laboratory frame of the reflected ions, is given by equating the pressure exerted by the laser with that exerted by the in-streaming and reflected ions, neglecting the electron inertia. Allowing for a reflected wave of intensity I^- , the energy-momentum tensor $T^{\mu\nu}$ of the radiation field has the following non-vanishing elements

$$\begin{aligned} T^{00} &= T^{11} = (I^+ + I^-) / c = I^+ (1 + R) / c \\ T^{01} &= T^{10} = (I^+ - I^-) / c = I^+ (1 - R) / c \end{aligned} \quad (2)$$

where the reflectivity is $R = I^-/I^+$. The front is assumed to move into the solid (which is at rest in the lab. frame) at constant speed $c\beta_f$, and the elements $T'^{\mu\nu}$ of the energy-momentum tensor of the laser in the rest-frame of the front (the “HB-frame”) follow from Lorentz boosting (2):

$$T'^{01} = T'^{10} = \Gamma_f^2 [(1 - \beta_f)^2 - (1 + \beta_f)^2 R] I^+ / c \quad (3)$$

$$T'^{00} = T'^{11} = \Gamma_f^2 [(1 - \beta_f)^2 + (1 + \beta_f)^2 R] I^+ / c \quad (4)$$

where $\Gamma_f = (1 - \beta_f^2)^{-1/2}$. Thus, the reflectivity in the rest frame of the hole-boring front is

$$R' = \left(\frac{1 + \beta_f}{1 - \beta_f} \right)^2 R \quad (5)$$

$$= D^{-4} R \quad (6)$$

where the Doppler factor

$$D = \left(\frac{1 - \beta_f}{1 + \beta_f} \right)^{1/2} \quad (7)$$

is the ratio of the laser frequency ω in the HB-frame to its value ω_{lab} in the lab. frame.

On the other hand, the elements of the energy-momentum tensor on the target side of the hole-boring front are found by assuming perfect reflection of the ions. In the HB-frame, therefore, two mono-energetic beams of velocity $\pm c\beta_f$ and proper density ρ exist immediately behind the front, so that

$$T'^{00} = 2\rho c^2 \Gamma_f^2 \quad (8)$$

$$T'^{11} = 2\rho c^2 \beta_f^2 \Gamma_f^2 \quad (8)$$

$$T'^{01} = 0 \quad (9)$$

The requirement that T'^{11} be continuous across the front determines the advance speed, provided R' is known:

$$\beta_f = \sqrt{\xi} / (1 + \sqrt{\xi}) \quad (10)$$

where the reflection-modified X parameter is defined as

$$\xi = X(1 + R')/2 \quad (11)$$

The Doppler factor and (dimensionless) x -component of the four-velocity of the front, $u_f = \beta_f \Gamma_f$, are also functions of ξ alone:

$$D = (1 + 2\sqrt{\xi})^{-1/2} \quad (12)$$

$$u_f = D\sqrt{\xi} \quad (13)$$

and the reflectivity in the lab. frame is

$$R = (1 + 2\sqrt{\xi})^{-2} R' \quad (14)$$

In the standard hole-boring scenario, perfect reflection is assumed in the rest frame of the hole-boring front: $R' = 1$, $\xi = X$, in which case these expressions agree with those given by [6]. In this case, the electric and magnetic fields, as seen in the HB-frame, form a standing wave. They are everywhere parallel, and lie in a plane that contains the x -axis and rotates about it. The field magnitudes are constant in time at each position, but at a given instant vary sinusoidally in x with equal amplitudes

$$E_{\text{ampl}} = 2D\sqrt{4\pi I^+/c} \quad (15)$$

and a phase difference of $\pi/2$. As we show below, a pair cushion greatly reduces R' , leading to a smaller speed of advance of the hole-boring front, and a reduced electric field amplitude.

3. Two-fluid model of the pair cushion

3.1. Governing equations

In the presence of a pair plasma, the incident and reflected waves in the excavated channel are strongly coupled, and the relevant solutions are not vacuum waves, but nonlinear, transverse electromagnetic modes of superluminal phase speed. We use a cold, two-fluid (electron and positron) description to analyze these waves. The continuous charge and current distributions are related to the fields by Maxwell's equations. The fluids obey equations of motion that contain not only the wave fields, but also the classical radiation reaction force, thus taking into account the discrete nature of the fluid constituents. The cartesian four-velocity components and the proper densities are denoted by $u_{x,y,z}^\pm$ and n^\pm . Since we treat circular polarization, it is convenient to use rotating coordinates:

$$u_\perp^\pm = u_y^\pm + iu_z^\pm \quad E = E_y + iE_z \quad B = B_y + iB_z \quad (16)$$

In order to find nonlinear solutions that are homogeneous in the y - z plane, we make a number of simplifications: Firstly, in the transverse electromagnetic waves of interest here, electrons and positrons have the same density and oppositely directed transverse momenta: $n^- = n^+ = n$ and $u_\perp^- = -u_\perp^+ = u_\perp$. It follows that $E_x = 0$. Secondly, we look for solutions which the fluids do not stream along x in the frame in which the hole-boring front is stationary: $u_x^\pm = 0$. In the following, the \pm notation is dropped and the equations presented apply to the electron fluid in this frame.

The classical radiation reaction force in the Lorentz-Abraham-Dirac formulation is:

$$g^\mu = \frac{2e^2}{3mc^3} \left(\frac{d^2 u^\mu}{d\tau^2} - u^\mu \left| \frac{du^\nu}{d\tau} \right|^2 \right) \quad (17)$$

and it is clear that the spatial components lie in the y - z plane when $u_x \equiv 0$. This property is shared by the Landau-Lifshitz formulation of radiation reaction, in which the derivatives in (17) are replaced using the Lorentz equation of motion (see [9] for a review). Thus, the x -component of the fluid equation of motion is unaffected by radiation reaction:

$$\left(\gamma \frac{\partial}{\partial t} + cu_x \frac{\partial}{\partial x} \right) u_x = - \frac{e}{mc} \text{Im}(u_\perp B^*) \quad (18)$$

where $\gamma = u^0$. Solutions with $u_x = 0$ for all x and t , therefore, require the transverse velocity and magnetic field vectors to be parallel:

$$\text{Im}(u_\perp B^*) = 0 \quad (19)$$

On the other hand, the (complex) equation of motion in the transverse plane contains a term due to radiation reaction:

$$\gamma \frac{\partial u_\perp}{\partial t} = - \frac{e}{mc} \gamma E + g_\perp \quad (20)$$

where g_\perp is the spatial part of g^μ in rotating coordinates, and we have set $u_x = 0$. For these transverse fields ($E_x = 0$, $B_x = 0$), the set of governing equations is completed by

the Faraday and Ampère equations:

$$\frac{\partial E}{\partial x} - \frac{i}{c} \frac{\partial B}{\partial t} = 0 \quad (21)$$

$$\frac{\partial B}{\partial x} + \frac{i}{c} \frac{\partial E}{\partial t} = i8\pi enu_{\perp} \quad (22)$$

and the equation of continuity:

$$\frac{\partial}{\partial t} (\gamma n) = 0 \quad (23)$$

3.2. Method of solution

We seek solutions that are separable in x and t in the HB-frame. In particular, for a monochromatic wave of angular frequency, ω , the quantities E , B , and u_{\perp} are proportional to $e^{i\omega t}$, whereas n and $|u_{\perp}|$ are constant in time. Since force balance along x (19) requires the fluid velocity to be parallel to the magnetic field, the complex variables E , B and u_{\perp} can be replaced by three real, positive, dimensionless amplitudes a , b and u , together with two phases, ϕ and δ , all of which are functions of x only:

$$E = \left(\frac{mc\omega}{e} \right) ae^{i\phi+i\omega t} \quad (24)$$

$$B = \left(\frac{mc\omega}{e} \right) ibe^{i\phi+i\delta+i\omega t} \quad (25)$$

$$u_{\perp} = iue^{i\phi+i\delta+i\omega t} \quad (26)$$

Substituting these into (20), the transverse equations of motion become:

$$u = a \cos \delta \quad (27)$$

$$\delta = \arctan(\epsilon u^3) \quad (28)$$

where

$$\epsilon = \frac{2}{3} \frac{\omega e^2}{mc^3} \quad (29)$$

$$= 1.18 \times 10^{-8} D \lambda_{\mu\text{m}}^{-1} \quad (30)$$

with $\lambda_{\mu\text{m}}$ the laser (vacuum) wavelength in the lab. frame in microns. The Lorentz-Abraham-Dirac form (17) of the radiation reaction term was used in deriving (28), and only the leading contribution in an expansion in $1/\gamma$ was retained:

$$g_{\perp} \approx - (2e^2\omega/3mc^3) \omega\gamma^4 u_{\perp} \quad (31)$$

The Landau-Lifshitz form yields exactly the same result in this limit.

The pair fluids do not contribute to the (1, 1) and (0, 1) components of the energy-momentum tensor. The latter is, therefore, just the Poynting flux:

$$\begin{aligned} T^{r01} &= \left(\frac{m^2 c^2 \omega^2}{8\pi e^2} \right) P \\ P &= 2ab \cos \delta \end{aligned} \quad (32)$$

and the former is the energy-density of the fields:

$$\begin{aligned} T'^{11} &= \left(\frac{m^2 c^2 \omega^2}{8\pi e^2} \right) U \\ U &= a^2 + b^2 \end{aligned} \quad (33)$$

The Faraday and Ampère equations take the form:

$$da/dx = b \sin \delta \quad d\phi/dx = -(b/a) \cos \delta \quad (34)$$

$$db/dx = -a \sin \delta \quad d\delta/dx = [(n - n_{\text{cr}})/n_{\text{cr}}] (a/b) \cos \delta - d\phi/dx \quad (35)$$

and can be used to evaluate the divergence (in this case, derivative with respect to x) of T'^{01} and T'^{11} :

$$\frac{dP}{dx} = -2 (n/n_{\text{cr}}) a^2 \sin \delta \cos \delta \quad (36)$$

$$\frac{dU}{dx} = 0 \quad (37)$$

where $n_{\text{cr}} = m\omega^2/8\pi e^2$ is the critical proper density.

The solution of the system (27), (28), (34) and (35) can be reduced to a quadrature:

$$x = \int d\delta \frac{4 - 3 \cos^2 \delta}{3 \sin^2 \delta \cos \delta} \left[\left(\frac{r_c \cos^4 \delta}{\sin \delta} \right)^{2/3} - 1 \right]^{-1/2} \quad (38)$$

where

$$r_c = \epsilon U^{3/2} = \text{constant} \quad (39)$$

Having found $\delta(x)$, a and u follow from (27) and (28). The constant pressure condition, (37), determines the magnetic field b in terms of the constant $a_0 = \sqrt{a^2 + b^2} = \sqrt{U}$ and the density follows from energy conservation, (36):

$$\frac{n}{n_{\text{cr}}} = \frac{2a^2 + 3a^2 \sin^2 \delta - a_0^2}{a^2 (4 - 3 \cos^2 \delta)} \quad (40)$$

Finally, the phase ϕ is evaluated from

$$\phi = - \int da \frac{\tan(\delta)}{a} \quad (41)$$

This solution depends on only one parameter, r_c , which determines the importance of radiation reaction, and is equivalent to R_C in the notation of de Piazza et al [9]. The ‘‘classical radiation-dominated regime’’ corresponds to $r_c > 1$. In terms of laser parameters,

$$r_c = 7.4 \lambda_{\mu\text{m}}^2 (I^+/10^{24} \text{ W cm}^{-2})^{3/2} D (1 + R')^{3/2}$$

3.3. Boundary conditions

At the downstream boundary, $x = x_2$, (see Fig. 1) the fields of the pair cushion must match those of either the hole-boring front or a vacuum gap. Continuity of the energy-momentum tensor components T'^{01} requires zero Poynting flux, because the hole-boring

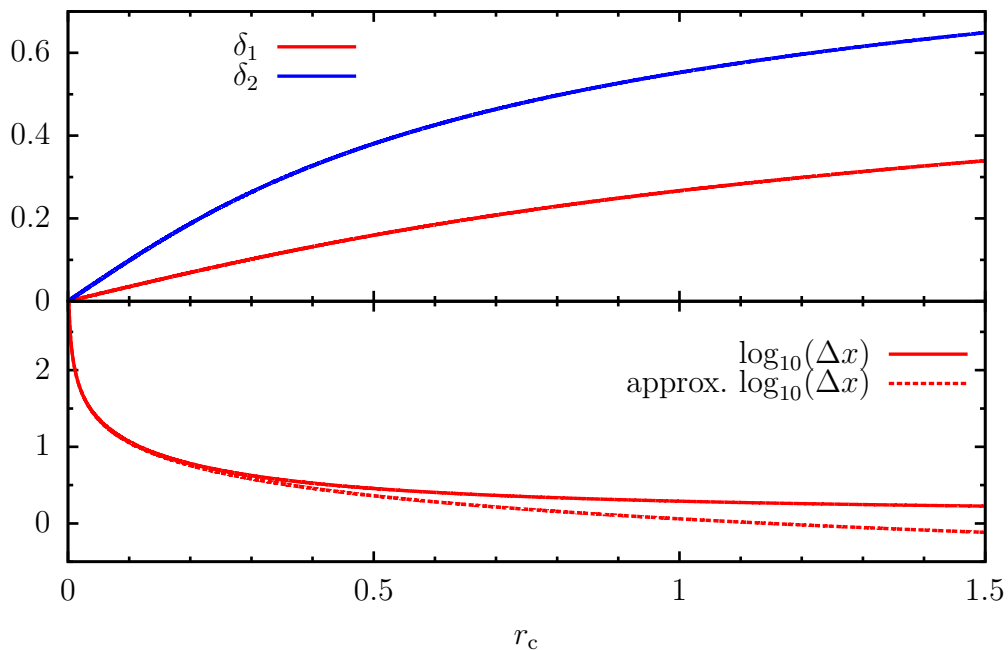


Figure 2. Top: the phase-shift of the magnetic field caused by radiation reaction at the upstream (δ_1) and downstream (δ_2) edges of the pair cushion (the angle between the electric and magnetic field vectors is $\pi/2 + \delta$). Bottom: the maximum thickness $\Delta x = x_2 - x_{\min}$ of the cushion (in units of c/ω) compared to the approximate expression (43), both as functions of the radiation reaction parameter r_c defined in (39)

front is assumed perfectly reflecting in the HB-frame. Using the notation $a_{1,2} = a(x_{1,2})$ etc., this implies either $b_2 = 0$, or $a_2 = u_2 = \delta_2 = 0$. The latter possibility is, however, unphysical, since it implies $da/dx > 0$ for $x \rightarrow x_2$, leading to a negative value of a just upstream of this boundary. Thus, $b_2 = 0$, $a_2 = a_0$, and δ_2 follows from (27) and (28). This means that the edge of the pair cushion cannot be located at the mirror, where continuity of the tangential component of E requires it to vanish. Because the finite-density cushion cannot carry a singular current sheet at the surface $x = x_2$, the transverse component of B must also be continuous across it. Therefore, this point lies at a node of the magnetic field not only of the plasma wave, but also of the standing wave that occupies the vacuum region $x > x_2$. The cushion must, therefore, be separated from the mirror by a vacuum gap of thickness $(j + 1/2)\pi c/\omega$, where $j = 1, 2, \dots$. According to (40), the pair density reaches the critical value at the edge of this gap: $n_2 = n_{\text{cr}}$.

At the upstream boundary, $x = x_1$, the fields in the cushion must match the vacuum fields of the incident and reflected laser beams. The location of this point is fixed by the number of pairs contained per unit area of the cushion, which rises with increasing cushion thickness from zero when $x_1 = x_2$ to a maximum value determined by the point at which the proper pair density vanishes. The electric field amplitude $a = a_{\min}$ at

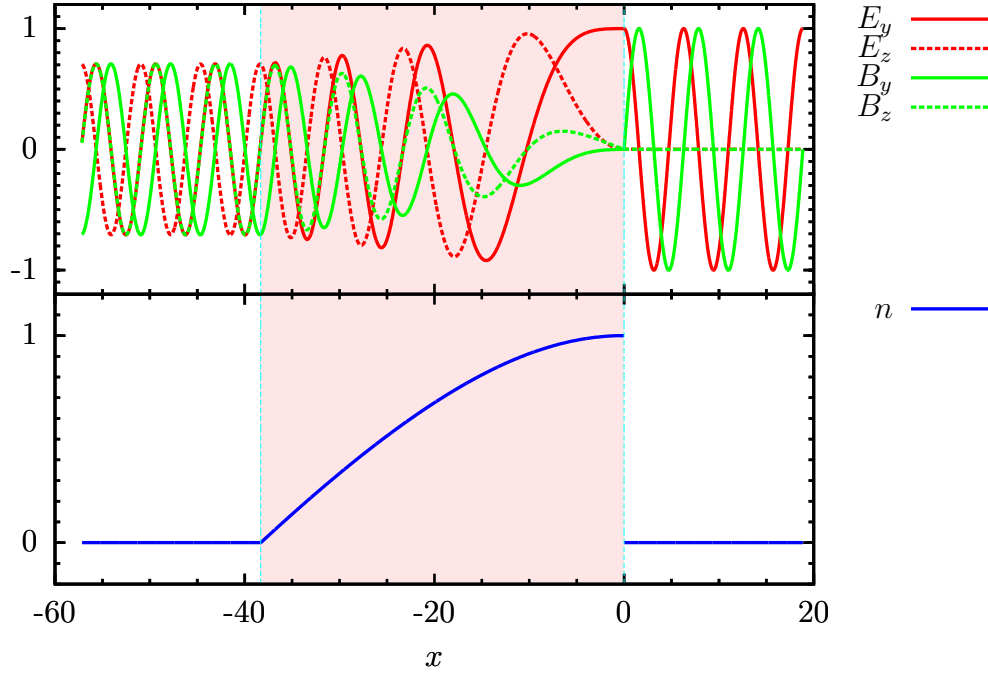


Figure 3. Top: the spatial profile of the electromagnetic fields, as seen in the rest frame of the hole-boring front at $t = 0$, normalized to the value $a_0 m c \omega / e$. Bottom: the proper density, normalized to the critical density $\omega^2 m / (8\pi e^2)$. The edges of the pair front are indicated by vertical lines at $x_1 = -38.3$ and $x_2 = 0$. Note that the fields are continuous, but the current-density discontinuity at $x = 0$, imposes a discontinuity on the x derivative of B (but not of E). In this figure, the radiation reaction parameter is $r_c = 0.03$.

which this occurs can be found from (27), (28) and (40):

$$\epsilon^2 (5a_{\min}^2 - a_0^2)^4 + 54a_{\min}^2 - 27a_0^2 = 0 \quad (42)$$

The corresponding position sets the maximum thickness, Δx (in units of c/ω), of the pair front compatible with a physically acceptable solution. In general, a quadrature is needed to find this quantity. However, for $r_c \ll 1$, one finds $\delta_2 \approx r_c$, $\delta_1 \approx r_c/2^{3/2}$, and $a_1 \approx a_0/\sqrt{2}$. This leads to the approximate expression:

$$\begin{aligned} \Delta x &= |x_2 - x_1|_{\max} \\ &\approx \frac{1}{r_c} \int_{1/\sqrt{2}}^1 \frac{dy}{y^3 \sqrt{1-y^2}} \\ &\approx 1.1478/r_c \end{aligned} \quad (43)$$

Fig 2 compares this result to the numerically evaluated quadrature.

4. Results

The spatial dependence of the electromagnetic fields is shown in Fig 3, for $r_c = 0.03$ at time $t = 0$ (the fields are proportional to $e^{i\omega t}$). In this example, the pair front has been chosen to have its maximum thickness, i.e., the density vanishes at the upstream edge. It then rises monotonically, reaching the critical value at the downstream edge of the front, where $x = 0$. For $r_c \ll 1$, the thickness of the front is large compared to the laser wavelength in vacuo, and it is easy to see that the fields belong to an oscillation whose wavelength grows as the pair density rises. The increase in wavelength corresponds to an increase of the phase-velocity of the wave $v_{\text{ph}} = \omega/k$, but a decrease of the group velocity $v_g = c^2k/\omega$, which vanishes at the downstream edge.

Although the complex fields are separable functions of x and t , their real components are not. This means that the solutions are not standing waves in the strict sense [10], except in the vacuum gap between the cushion and the target, where the Poynting flux vanishes. However, they can easily be visualized as a stationary structure that rotates about the x -axis. This structure forms a helix or screw thread of variable pitch. Upstream of the cushion, the pitch is almost constant, but with a small periodic fluctuation due to the finite amplitude of the reflected wave. Inside the cushion, the pitch increases monotonically with the pair density, becoming infinite at the downstream edge, where $n_2 = n_{\text{crit}}$.

Vacuum waves propagate both upstream and downstream of the pair front. Upstream (the region $x < 38.3$ in Fig. 3), the amplitude of the backward propagating wave is given by the reflectivity of the overall system consisting of pair front plus hole-boring front. For a pair front of maximum thickness,

$$R' = \frac{a_0^2 - 2a_1b_1 \cos \delta_1}{a_0^2 + 2a_1b_1 \cos \delta_1} \quad (44)$$

and, assuming $r_c \ll 1$, one finds

$$\begin{aligned} R' &\approx \delta_1^2/4 \\ &\approx r_c^2/32 \end{aligned} \quad (45)$$

For the parameters of Fig. 3, $R' \approx 2.8 \times 10^{-5}$, and the forward propagating wave dominates, so that $E_y \approx B_z$ and $E_z \approx -B_y$.

Downstream of the pair front, where $x > x_2$, the forward and backward propagating waves are of equal magnitude, since the hole-boring front is assumed to be perfectly reflecting. Here, the electric and magnetic fields are everywhere parallel. At $t = 0$, they are directed along the y axis, and rotate together in a clockwise sense, when viewed along the positive x -direction.

At both the upstream and downstream edges, the electromagnetic fields are continuous, as are the fluxes of energy, T'^{01} , and x -momentum, T'^{11} . The density, however, is discontinuous (note that $u_x = 0$), although only at the downstream edge for a front of maximum permitted thickness. A discontinuity in the density implies a

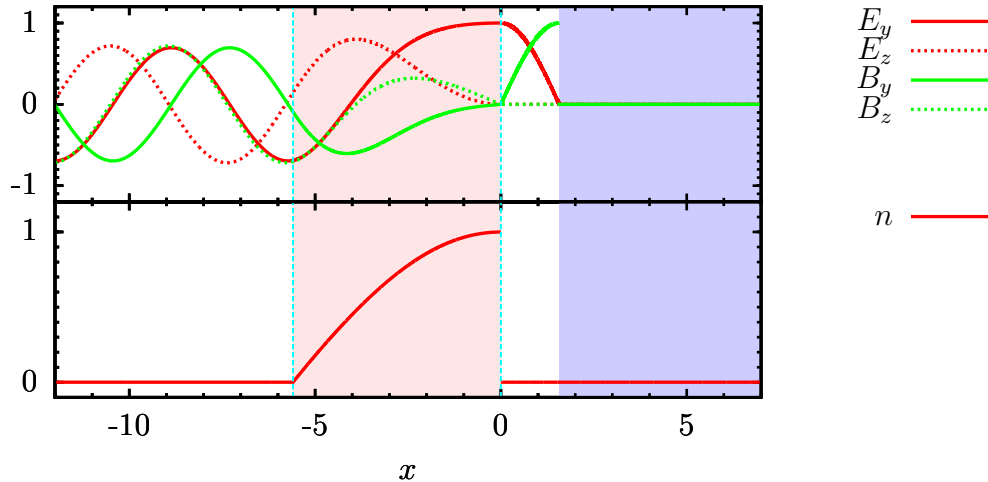


Figure 4. The field and pair density profiles in the presence of a pair cushion. (shaded red) for $r_c = 0.2$. The target is shaded blue. The boundaries of the pair cushion are at $x_1 = -5.6$ and $x_2 = 0$.

discontinuity also in the current density. As a result, the x -derivative of the magnetic field has a discontinuity, but that of the electric field does not.

The edge of the pair cushion at $x = x_2$ is located at a node of the magnetic field in the standing wave that lies downstream of it. The hole-boring front itself, however, can be located at any of the nodes of the electric field in this wave. Choosing the minimum vacuum gap size, the fields in the pair cushion and vacuum gap are illustrated in Fig. 4, for $r_c = 0.2$.

5. Applications

When the pair front contains very few particles, $b_1 \rightarrow b_2 = 0$ and the reflectivity approaches its maximum value, which is that of the standard scenario without a pair front, $R' = 1$, $R = 1 / \left(1 + 2\sqrt{X}\right)^{-2}$. However, the minimum value of R' , which is attained for the maximum number of pairs consistent with a stationary solution, depends on the radiation reaction parameter r_c , which, in turn, depends not only on the hole-boring parameter X , but also on the laser wavelength and the number of pairs contained in the cushion.

As an example, we consider the effect of a pair cushion when an intense laser pulse of wavelength $\lambda_{\mu\text{m}} = 1$ impacts an aluminium target ($\rho = 2.7 \times 10^3 \text{ kg m}^{-3}$, $Z = 13$). This target is over-dense, since the ratio of the electron density to the critical density is $698 \lambda_{\mu\text{m}}^2$. Therefore, the hole-boring scenario can be expected to apply provided the laser is not intense enough to render it relativistically under-dense, which implies the restriction $I_{24} < 1.33 \lambda_{\mu\text{m}}^2$, assuming a circularly polarized pulse. For laser intensities in this range, the stationary solution with the largest number of pairs is found by iteratively

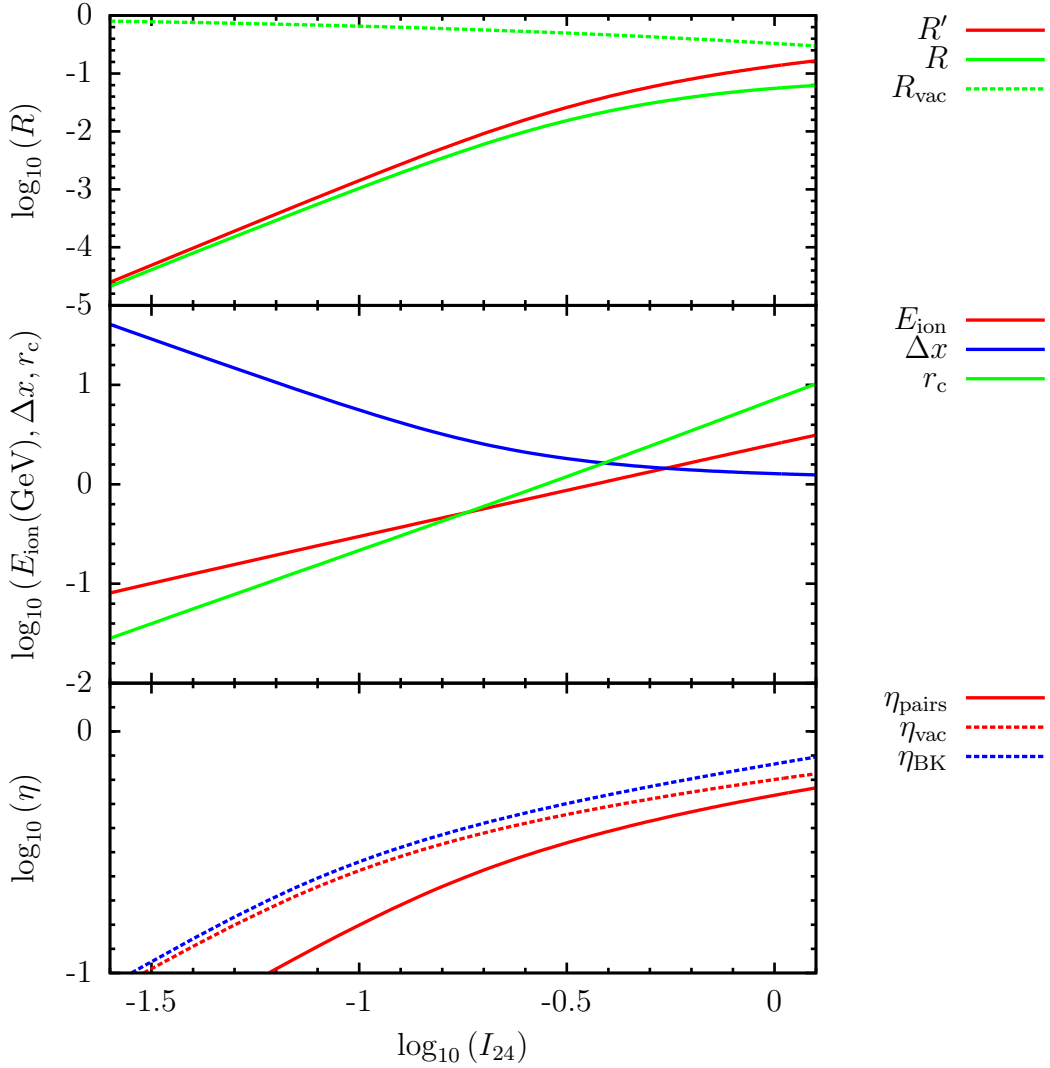


Figure 5. As functions of the laser intensity $I_{24} \times 10^{24} \text{ W cm}^{-2}$, for a wavelength of $1 \mu\text{m}$ and an aluminium target:

Top panel: The reflectivity R in the lab. frame and R' in the frame of the hole-boring front when a pair front of maximal extent is present. For comparison, the reflectivity R_{vac} in the lab. frame in the absence of a pair front is also shown.

Centre panel: The kinetic energy in the lab. frame E_{ion} of an ion reflected into the target by the hole-boring front, the thickness of the pair cushion, in units of c/ω , and the parameter r_c characterizing the strength of classical radiation reaction.

Bottom panel: The non-linear QED parameter reached by electrons and positrons in the pair front for maximal suppression due to absorption of the laser by the pair front, η_{pairs} and for negligible absorption η_{vac} . For comparison, the quantity η_{BK} , as given by [4], is plotted. This applies to counter-propagating laser beams, each of the given intensity, in an under-dense plasma.

solving (10) and (11) together with (44).

The top panel of Fig. 5 shows the reflectivities in the lab. and hole-boring frames assuming a pair front of maximum extent is present in the channel. At low intensities, the laser is almost completely absorbed by the pair cushion. In the approximation used to describe radiation reaction, (31), the energy absorbed is converted entirely into transversely directed, synchrotron-like radiation. Thus, in the HB-frame the efficiency of conversion of laser light into high energy photons is $1 - R'$, i.e., close to 100% at low intensities and 87% at an intensity of $10^{24} \text{ W cm}^{-2}$.

The middle panel of Fig. 5 shows the kinetic energy in the lab. frame of an aluminium ion reflected back into the target off the advancing hole-boring front: $E_{\text{ion}} = 2Mc^2\beta_f^2\Gamma_f^2$. In the case shown here, the speed of advance of the hole-boring front $c\beta_f$, remains non-relativistic, even for the highest intensity plotted. It is assumed here that, for a given laser intensity, the pair cushion attains its maximum possible thickness, which is plotted in units of c/ω as a function of laser intensity in this panel. Also shown is the parameter r_c which characterizes the importance of the classical radiation reaction force. Above $I \approx 3 \times 10^{23} \text{ W cm}^{-2}$, this parameter exceeds unity, i.e., the energy radiated by a single electron or positron in one laser period is greater than the particle energy. Radiation reaction is responsible for the change in slope at roughly this intensity of the curves depicting R' and R in the upper panel. When quantum effects are small (see lower panel) the synchrotron-like radiation emitted at the downstream edge of the cushion peaks at an energy

$$h\nu_\gamma \approx 0.7mc^2 (r_c/\alpha_f) \cos^3 \delta_2 \quad (46)$$

where α_f is the fine-structure constant.

The lower panel of Fig. 5 plots the the QED parameter η , the ratio of the electric field seen in the electron or positron rest frame to the critical field $E_c = m^2c^3/e\hbar$ at the edge of the pair front. As η approaches unity, quantum effects such as electron recoil on emitting a photon and pair production begin to become important. Three curves are shown. At low intensities, where the number of pairs that can be contained in a stationary cushion is relatively large, the solid red line (depicting η in the presence of a maximal pair cushion) lies well below the dashed red line (depicting η in the absence of a pair cushion.) At intensities close to $10^{24} \text{ W cm}^{-2}$, the reduction is less marked, being roughly 15%. Both of these curves lie below that predicted for counter-propagating vacuum waves of intensity I^+ [4], shown as a blue dashed line. This is because of the recoil of the target, which effectively reduces the pressure and frequency of the incident laser pulse [2]. Assuming $a_0 \gg 1$, we find

$$\eta_{\text{pairs}} = (\hbar\omega/mc^2) a_0^2 \cos^2 \delta_2 \quad (47)$$

At low intensity, $\eta_{\text{pairs}} \propto a_0^2 \propto \sqrt{I^+}$, but the factor $\cos^2 \delta$, arising from the phase shift between the force on the charged fluids and the electric field which is brought about by radiation reaction, causes η to rise less rapidly with laser intensity when $I^+ > 3 \times 10^{23} \text{ W cm}^{-2}$ [4].

6. Discussion

The solutions presented above fulfil the fully nonlinear coupled fluid and Maxwell equations including radiation reaction. Several studies have treated classical radiation reaction in the contexts of the hole-boring scenario and of counter-propagating laser beams [11, 12, 13], but these neglect the influence of the radiating particles on the laser fields. Classical radiation reaction terms have been incorporated in particle-in-cell simulation codes, which, in principle, treat the fields self-consistently [8, 14, 15]. However, the solutions we find are analytical, in the sense that they can be reduced to the quadratures (38) and (41). This makes them a useful and flexible tool for the interpretation of both simulations and experiments.

The unique aspect of these solutions is the inclusion of classical radiation reaction. This force, acting on a single charged (relativistic) particle moving in the coherent laser field, is approximately anti-parallel to the particle speed in the lab. frame. The energy dissipated is carried off primarily as short-wavelength photons. We assume the fluids in our treatment consist of electrons and positrons that radiate independently of each other, which is reasonable provided the wavelength of the radiated photons in the particle rest-frame is small compared to the inter-particle spacing in that frame. For photons of frequency $a_0^3 \omega_{\text{lab}}$ close to the peak of the synchrotron-like spectrum and for a pair plasma at the critical density, this ratio can be estimated as

$$\begin{aligned} \varepsilon &= \frac{c / (a_0^2 \omega_{\text{lab}})}{(4\pi e^2 / m \omega_{\text{lab}}^2)^{1/3}} \\ &= (a_0^3 r_c)^{-1/3} \\ &= 6 \times 10^{-4} D^{-1/3} (1 + R')^{-1} \lambda_{\mu\text{m}}^{-5/3} (I^+ / 10^{24} \text{ W cm}^{-2})^{-1} \end{aligned} \quad (48)$$

so that our approach is justified for optical lasers with $I^+ > 10^{21} \text{ W cm}^{-2}$.

In this regime, classical radiation reaction introduces an effective friction term into the equations of motion for the fluids. For the one-dimensional problem considered here, this force lies in the y - z plane and has no component in the direction of laser propagation. As a result, the pair cushion remains in place provided the pressure in the electromagnetic fields of the laser, $(E^2 + B^2)/8\pi$, remains constant. On the other hand, energy conservation requires that the Poynting flux in the cushion decrease monotonically towards the target. This is achieved by allowing $|B|$ to decrease, reaching zero at the front edge of the cushion, which, therefore, matches to a node of the magnetic field in the standing wave that separates it from the target.

As noted in section 3, the effective friction force does not depend on which of the Lorentz-Abraham-Dirac or the Landau-Lifshitz formulations of the radiation reaction term is used. The underlying reason is that we have treated only stationary solutions of the equations. An investigation of the stability properties of the solutions, on the other hand, can be expected to reveal a difference.

However, our results should also be modified by quantum effects. When $\eta_{\text{pairs}} \sim 1$, the characteristic energy of the radiated photons is comparable to that of the radiating

particle. In this case losses become a discrete process, and cannot be represented by a “smooth” friction term. As is well-known in the analogous case of betatron oscillations, this is likely to have a strong influence on the stability properties of the solutions [16]. But, even before the discrete nature becomes pronounced, quantum effects significantly reduce the time-averaged energy loss rate. For example, when $\eta \approx 1/10$, an emitted photon takes off only 10% of the particle energy, but the time-averaged energy loss rate is reduced by a factor of 1/3. This reduction can be accounted for in an approximate manner by modifying the radiation reaction term [17]. Using this approach, it would be possible to improve the rough estimate (46) of the energy spectrum of the emitted gamma-rays, although this would necessitate a more elaborate numerical solution.

In common with all analytical solutions, those we present above suffer from several limitations. For low laser intensities, the linear extent of the maximal cushion becomes large (see Fig. 5), so that the stationary solution can be realized only for a rather long incident pulse. Also, it is not clear that a significant number of pairs will be available to form a cushion in a realistic experimental configuration, particularly at low laser intensity. At high intensity, on the other hand, the underlying hole-boring scenario itself is in doubt. Piston oscillations can become pronounced, and hot electrons may leak from the target into the vacuum gap [6, 7, 8]. Eventually, even solid targets become relativistically under-dense and are unable to reflect the incident pulse. In Fig. 5 we have implicitly adopted the conventionally estimated threshold for this effect, although possible departures from it have been discussed in the literature [18, 19, 20].

7. Conclusions

We present solutions to the coupled set of Maxwell’s equations and those for two cold, charged, relativistic fluids (pair plasma), including classical radiation reaction. The pair plasma reaches critical density and is bounded by regions containing vacuum fields: an incident laser and its reflected beam on one side, and a standing vacuum wave separating the pair plasma or “cushion” from an over-dense target on the other. The solutions have two main properties, both of which are shown in Fig. 5: First, the pair cushion forms an efficient device for converting the energy flux in the laser into high energy photons, as is evident from the substantial reduction in the reflectivity. Second, the laser intensity at which quantum effects become important is increased somewhat, as can be seen from the difference between η_{pairs} and η_{vac} .

However, it is not possible, using our calculations, to make a reliable estimate of the threshold for the onset of a nonlinear pair cascade, since important effects such as “straggling” [21] are not considered.

Acknowledgments

ARB and CPR thank the UK Engineering and Physical Sciences Research Council for support under grant EP/G055165/1.

References

- [1] E. N. Nerush, I. Y. Kostyukov, A. M. Fedotov, N. B. Narozhny, N. V. Elkina, and H. Ruhl. Laser Field Absorption in Self-Generated Electron-Positron Pair Plasma. *Physical Review Letters*, 106(3):035001, January 2011.
- [2] C. P. Ridgers, C. S. Brady, R. Ducloux, J. G. Kirk, K. Bennett, T. D. Arber, A. P. L. Robinson, and A. R. Bell. Dense Electron-Positron Plasmas and Ultraintense γ rays from Laser-Irradiated Solids. *Physical Review Letters*, 108(16):165006, April 2012.
- [3] C. S. Brady, C. P. Ridgers, T. D. Arber, A. R. Bell, and J. G. Kirk. Laser Absorption in Relativistically Underdense Plasmas by Synchrotron Radiation. *Physical Review Letters*, 109(24):245006, December 2012.
- [4] A. R. Bell and J. G. Kirk. Possibility of Prolific Pair Production with High-Power Lasers. *Physical Review Letters*, 101(20):200403–+, November 2008.
- [5] A. M. Fedotov, N. B. Narozhny, G. Mourou, and G. Korn. Limitations on the Attainable Intensity of High Power Lasers. *Physical Review Letters*, 105(8):080402, August 2010.
- [6] A. P. L. Robinson, P. Gibbon, M. Zepf, S. Kar, R. G. Evans, and C. Bellei. Relativistically correct hole-boring and ion acceleration by circularly polarized laser pulses. *Plasma Physics and Controlled Fusion*, 51(2):024004, February 2009.
- [7] T. Schlegel, N. Naumova, V. T. Tikhonchuk, C. Lobaune, I. V. Sokolov, and G. Mourou. Relativistic laser piston model: Ponderomotive ion acceleration in dense plasmas using ultraintense laser pulses. *Physics of Plasmas*, 16(8):083103, August 2009.
- [8] N. Naumova, T. Schlegel, V. T. Tikhonchuk, C. Lobaune, I. V. Sokolov, and G. Mourou. Hole Boring in a DT Pellet and Fast-Ion Ignition with Ultraintense Laser Pulses. *Physical Review Letters*, 102(2):025002, January 2009.
- [9] A. Di Piazza, C. Müller, K. Z. Hatsagortsyan, and C. H. Keitel. Extremely high-intensity laser interactions with fundamental quantum systems. *Reviews of Modern Physics*, 84:1177–1228, July 2012.
- [10] J. H. Marburger and R. F. Tooper. Nonlinear optical standing waves in overdense plasmas. *Physical Review Letters*, 35:1001–1004, October 1975.
- [11] S. V. Bulanov, T. Z. Esirkepov, M. Kando, J. K. Koga, and S. S. Bulanov. Lorentz-Abraham-Dirac versus Landau-Lifshitz radiation friction force in the ultrarelativistic electron interaction with electromagnetic wave (exact solutions). *Phys. Rev. E*, 84(5):056605, November 2011.
- [12] G. Lehmann and K. H. Spatschek. Phase-space contraction and attractors for ultrarelativistic electrons. *Phys. Rev. E*, 85(5):056412, May 2012.
- [13] T. Schlegel and V. T. Tikhonchuk. Classical radiation effects on relativistic electrons in ultraintense laser fields with circular polarization. *New Journal of Physics*, 14(7):073034, July 2012.
- [14] R. Capdessus, E. d’Humières, and V. T. Tikhonchuk. Modeling of radiation losses in ultrahigh power laser-matter interaction. *Phys. Rev. E*, 86(3):036401, September 2012.
- [15] B. Cerutti, G. R. Werner, D. A. Uzdensky, and M. C. Begelman. Simulations of Particle Acceleration beyond the Classical Synchrotron Burnoff Limit in Magnetic Reconnection: An Explanation of the Crab Flares. *Astrophysical J.*, 770:147, June 2013.
- [16] I. M. Ternov. REVIEWS OF TOPICAL PROBLEMS: Synchrotron radiation. *Physics Uspekhi*, 38:409–434, April 1995.
- [17] J. G. Kirk, A. R. Bell, and I. Arka. Pair production in counter-propagating laser beams. *Plasma Physics and Controlled Fusion*, 51(8):085008, August 2009.
- [18] F. Cattani, A. Kim, D. Anderson, and M. Lisak. Threshold of induced transparency in the relativistic interaction of an electromagnetic wave with overdense plasmas. *Phys. Rev. E*, 62:1234–1237, July 2000.
- [19] S. M. Weng, M. Murakami, P. Mulser, and Z. M. Sheng. Ultra-intense laser pulse propagation in plasmas: from classic hole-boring to incomplete hole-boring with relativistic transparency. *New Journal of Physics*, 14(6):063026, June 2012.

- [20] E. Siminos, M. Grech, S. Skupin, T. Schlegel, and V. T. Tikhonchuk. Effect of electron heating on self-induced transparency in relativistic-intensity laser-plasma interactions. *Phys. Rev. E*, 86(5):056404, November 2012.
- [21] R. Duclous, J. G. Kirk, and A. R. Bell. Monte Carlo calculations of pair production in high-intensity laser-plasma interactions. *Plasma Physics and Controlled Fusion*, 53(1):015009, January 2011.